Available online at www.sciencedirect.com

ScienceDirect

Geochimica et Cosmochimica Acta 328 (2022) 168–184

Geochimica et Cosmochimica Acta

www.elsevier.com/locate/gca

Vanadium isotope fractionation during hydrothermal sedimentation: Implications for the vanadium cycle in the oceans

Fei Wu [a,b,*], Jeremy D. Owens [b], Christopher R. German [c], Rachel A. Mills [d], Sune G. Nielsen [c,e]

[a] School of Earth Sciences, State Key Laboratory of Geological Processes and Mineral Resources, China University of Geosciences, Wuhan 430074, China

[b] Department of Earth, Ocean and Atmospheric Science and National High Magnet Field Laboratory, Florida State University, Tallahassee, FL, USA

[c] Department of Geology and Geophysics, Woods Hole Oceanographic Institution, Woods Hole, MA, USA

[d] University of Sussex, Brighton, United Kingdom

[e] NIRVANA Laboratories, Woods Hole Oceanographic Institution, Woods Hole, MA, USA

Received 21 November 2021; accepted in revised form 2 May 2022; available online 11 May 2022

Abstract

Variations of V isotope ratios ($\delta^{51}V$) in sedimentary rocks have been proposed as a potential proxy for paleo-oceanic redox conditions, although the marine $\delta^{51}V$ system is not fully constrained. Hydrothermal sediments are known to be a significant sink of V from the ocean. However, the V isotope fractionation associated with the accumulation into hydrothermal sediments from seawater and its influence on the marine isotopic budget of V are still unexplored. This work presents the first V isotope study of hydrothermal sediments specifically samples from the Trans-Atlantic Geotraverse (TAG) hydrothermal field and Pacific Ocean under influence of the hydrothermal plume arising from the southern East Pacific Rise (SEPR). The studied sediments show authigenic $\delta^{51}V$ values ranging from −0.4 to −0.1‰, which is remarkably different from that of non-hydrothermal oxic sediments (−1.2 to −0.7‰) as well as open ocean seawater (+0.2‰). The V isotope composition of these hydrothermal sediments at TAG is likely controlled by the isotope fractionation during the rapid initial uptake of V from seawater into hydrothermal Fe oxyhydroxide particulates that precipitate when reducing hydrothermal fluids mix with oxic seawater. The sediments collected from the deep south Pacific Ocean west of SEPR show authigenic $\delta^{51}V$ values overlapping with the range observed within the TAG field, despite their distal location extending to more than 4000 km from the buoyant portion of the SEPR hydrothermal plume. As has also been observed for Fe in particulates west of the SEPR, our results indicate the persistence of V within hydrothermal particulates (likely in the form of V-rich Fe oxyhydroxides) that settle to the sediments after long-range transport, while still preserving the original V isotope signature. Combination of this work with previous studies, allows us to establish a more robust mass balance model that assesses the effect of V removal by hydrothermal precipitation on the marine elemental and isotopic budget of V. Our new results suggest that the flux of V into the hydrothermal sink accounts for ~13% of the global marine V input. This model also indicates that the V isotope composition of seawater could potentially be altered with variations in hydrothermal activity which is in addition to changes

* Corresponding author at: School of Earth Sciences, State Key Laboratory of Geological Processes and Mineral Resources, China University of Geosciences, Wuhan 430074, China.

E-mail address: wufei@cug.edu.cn (F. Wu).

https://doi.org/10.1016/j.gca.2022.05.002

in the global marine redox conditions but likely on very different time scales. Thus, V isotope ratios have the potential to provide new insights into ancient ocean chemistry.

Keywords: V isotope; Metalliferous sediments; Hydrothermal plume; Oceanic V budget; Mass balance

1. INTRODUCTION

Vanadium (V) is a transition metal that can be found in four oxidation states (V^{5+}, V^{4+}, V^{3+}, and V^{2+}) in nature. Vanadium has two long-lived isotopes (^{51}V and ^{50}V) with relative abundances of ~99.76% and ~0.24%, respectively. With the development of high-precision measurements of V isotope ratios, the natural isotopic variations for vanadium have been explored in the last decade (Nielsen et al., 2011, 2016; Prytulak et al., 2011; Wu et al., 2016; Schuth et al., 2017; Dong et al., 2021). Recent studies have documented remarkable V isotope variations in marine sediments deposited under different redox conditions (Wu et al., 2019a, 2020; Chen et al., 2021), which are isotopically lighter than homogenous seawater value (Schuth et al., 2019; Wu et al., 2019b). The variable isotope fractionation of V during its scavenging from seawater and accumulation in marine sediments is likely controlled by the transition among V species with different valence states and solubility as a function of different redox environments, and mineral adsorption processes (Wu et al., 2015, 2019a, 2020). Recent observations indicate the strong linkage between authigenic marine sedimentary V isotope compositions and the overlying local redox conditions, which implies the potential application of V isotopes in seawater to track past variations in the extent of low oxygen environments (Wu et al., 2020; Fan et al., 2021; Nielsen, 2021).

The main species of V in oxic seawater is pentavalent vanadate (HVO_4^{2-} and $H_2VO_4^-$; Lewan and Maynard, 1982) with high solubility. Thus, in the modern oxic ocean, V behaves as a conservative element with a long residence time (~90 kyr, Nielsen, 2021), and shows invariant concentration and isotope composition in deep seawater (e.g. Ho et al., 2018; Wu et al., 2019b). Our current knowledge of the supply of V to the ocean is exclusively through riverine fluxes (Shiller and Mao, 2000; Nielsen, 2021), whereas removal of V from the ocean is mainly controlled by three principal vectors: (1) oxic sediments via adsorption to Fe and Mn oxides (e.g. Morford and Emerson, 1999); (2) incorporation into organic matter under reducing conditions in the water column leading to enrichments in underlying sediments (e.g. Wu et al., 2020); and (3) incorporation into hydrothermal particulates that form sediments at various distances from vents (e.g. Trefry and Metz, 1989) (Fig. 1). Previous studies have characterized V isotope compositions of the first two fluxes (Wu et al., 2019a; Wu et al., 2020), but hydrothermal sediments have yet to be studied for V isotopes (Fig. 1). It is important to have a complete characterization of V isotope variations in all these marine sediments in order to have a comprehensive understanding of the marine V isotope system.

The chemical compositions of hydrothermal vent fluids discharging from the seafloor at ocean ridges are quite different from that of seawater (e.g. Edmond et al., 1979; Wheat et al., 2002). In the modern ocean, a suite of sulfide and oxide phases form when the vent-derived fluids rapidly mix with cold, oxygenated seawater, which can scavenge numerous particle-reactive trace elements from ambient seawater (e.g. German et al., 1991; Feely et al., 1996). Hydrothermal alteration processes do not cause discernible changes in rock V concentrations or isotope compositions (Prytulak et al 2013; Wu et al., 2018), which implies that hydrothermal fluids only contain small amounts of V before mixing with seawater. On the other hand, multiple studies have documented that V co-precipitation with Fe-oxyhydroxides in hydrothermal plumes results in a net sink of marine V (Trefry and Metz, 1989; German et al., 1991). In the modern ocean, the net sink of V associated with hydrothermal deposits has been suggested to account for between 10% and 70% of the riverine influx of V (Trefry and Metz, 1989; Rudnicki and Elderfield,1993; Nielsen, 2021). Although with high uncertainty, it is clear that hydrothermal activity at mid-ocean ridges plays a critical role in the chemical budget of V in the ocean, which underlines the importance of determining the V isotope compositions of hydrothermal sediments and the mechanisms controlling these.

Here, we report V isotope data for metalliferous sediments from the Trans-Atlantic Geotraverse (TAG) hydrothermal field and sediments collected along the GEOTRACES East Pacific Zonal Transect (EPZT, GP16) that extended from the southern East Pacific Rise (SEPR) and more than 4000 km to the west. The controlling factor of V isotope fractionation during its coprecipitation with Fe oxyhydroxides and later burial into hydrothermal sediments from seawater will be discussed. Using these new data, an oceanic mass balance model of V is further developed, which provides constraints on the influence of hydrothermal V fluxes on the elemental and isotopic budget of V in the modern ocean. We also discuss possible V isotope variation of seawater as a function of changing global seawater chemistry and, thus, sedimentary V fluxes.

2. SAMPLE LOCALITIES AND BACKGROUND

The TAG hydrothermal field is located at 26°08′N on the slow-spreading mid-Atlantic ridge (MAR) and occupies ~100 km^2 on the east wall of the MAR rift valley (Fig. 2). Hydrothermal deposits consisting of active and relict sulfide mounds and Fe-Mn–oxides are found in this field between 2300 and 4000 m water depth. Three main zones of sulfide deposits have been mapped, including the actively venting

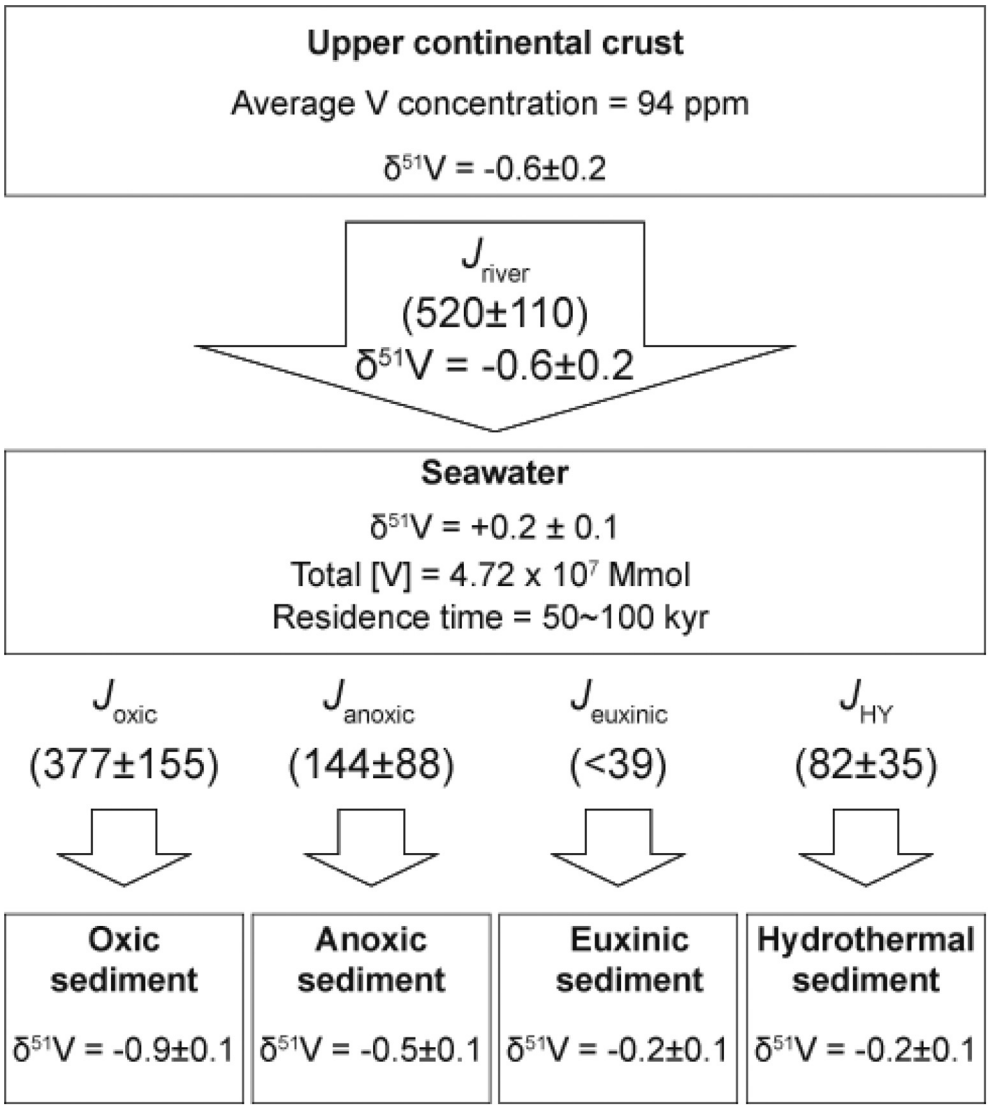

Fig. 1. Schematic summary of the oceanic V cycle modified from Nielsen (2021). The average concentration of V in upper continental crust is from Rudnick and Gao (2003). J_i (Mmol/yr) are the source and sink fluxes of V coming from Morford and Emerson (1999), Shiller and Mao (2000), Nielsen (2021), and this study. $\delta^{51}V$ (‰) of each reservoir are from Schuth et al. (2019), Wu et al. (2019a), Wu et al. (2020), and this study.

TAG mound and two fossil high-temperature vent fields known as the Mir zone and the Alvin zone (Rona et al., 1993). The currently active TAG mound is located at a depth of ~3670 m, near the foot of the eastern wall of the median valley within the TAG hydrothermal field (Fig. 2). Sediment formation in the TAG hydrothermal field is controlled by various styles of venting (high temperature focused or low temperature diffuse) and plume fallout and mass wasting of mound material (e.g., Thompson et al., 1985; Metz et al., 1988; German et al., 1993; Mills et al., 1993). Shallow (<15 cm depth) metalliferous sediments from the TAG hydrothermal field (on and off the currently venting mound) were selected for this study (Fig. 2 and Table 1). The metalliferous sediments on the TAG mound mainly consist of Fe sulfides and Fe-Mn oxides (German et al., 1993; Goulding et al., 1998), whereas the core-top metalliferous sediments off the TAG mound are formed by mixtures of fine-grained calcareous ooze, clay, and Fe-oxides (Metz et al., 1988; Mills et al., 1993).

Sediment collected during the US GEOTRACES East Pacific Zonal Transect (EPZT, GP16) were selected for this study. The hydrothermal plume components within the water column, especially Fe and Mn, sourced from SEPR are demonstrated to extend >4000 km west across the deep South Pacific Ocean carried by the westward-flowing mid-depth circulation (Resing et al., 2015; Fitzsimmons et al., 2017). Previous works have also shown that there were strong hydrothermal signals in sediments west of the SEPR (e.g. Barrett et al., 1987). The EPZT GP16 sediments are all pristine core-top samples that allow us to relate the sedimentary geochemical signature directly to the observed transport of the hydrothermal particulates in the South

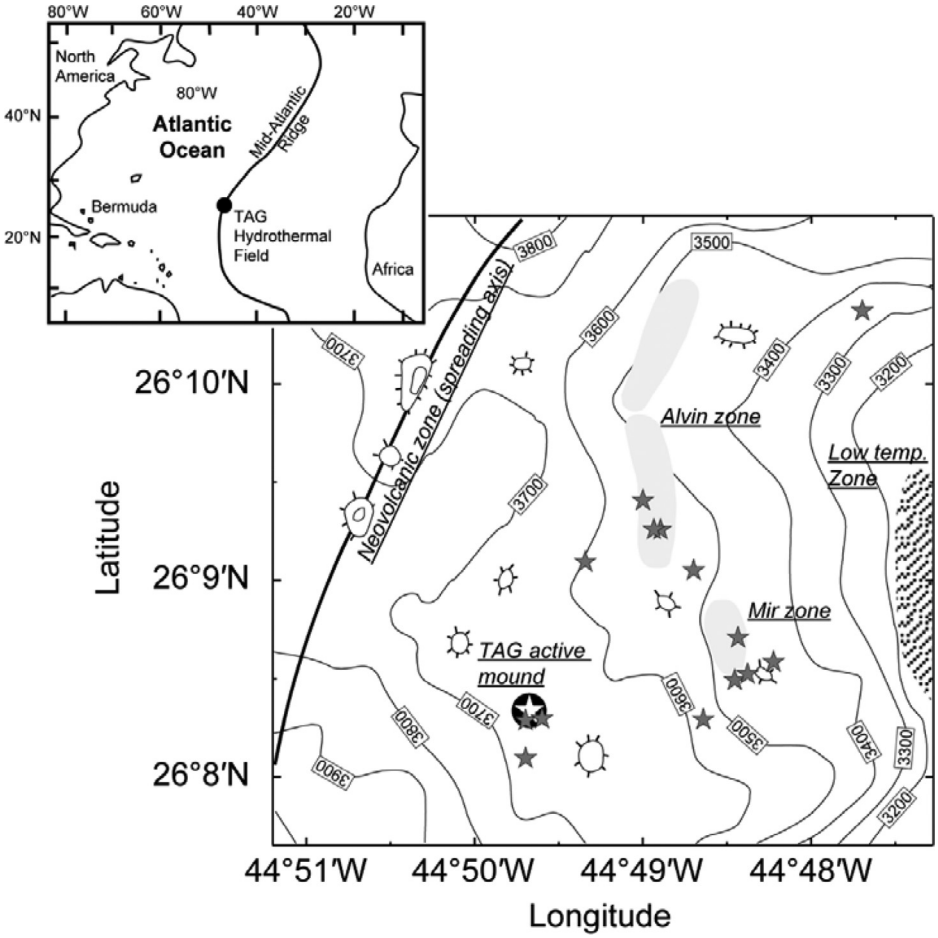

Fig. 2. Map of the 26°N TAG hydrothermal field showing active and inactive mounds. Grey stars denote the sampling location of the metalliferous sediments. Map is modified after Severmann et al. (2006). Bathymetric contour intervals are in meters.

Pacific Ocean. Wu et al. (2020) reported the V isotope composition of EPZT GP16 core top sediments between 77°W and 110°W longitude, to the east of the SEPR that do not have any influence of SEPR hydrothermal input. In this work, the EPZT GP16 sediments deposited between 113°W and 153°W longitude, to the west of the 15°S SEPR, were selected for V isotope study (Fig. 3 and Table 1). These samples are bulk powders representing the top 0–1 cm in each location.

3. METHODS

3.1. Sample dissolution

For metalliferous sediments from TAG hydrothermal field, approximately 5–40 mg of sample powders containing a total of at least 2 μg of V were digested for V isotope analysis. Samples were treated in combination with aqua regia and multi-acid HF–HNO_3–HCl procedure using trace metal clean acids, to ensure all the oxide and silicate phases were totally digested as described in Wu et al. (2019b). The EPZT GP16 sediments were dissolved using both bulk digestion and leaching methods to ensure that the V isotope analyses captured the the signatures directly extracted from seawater (authigenic fraction) rather than that from detrital fraction, given the limited enrichment of V for most of the samples. The bulk digestion was similar to that for TAG sediments. The procedure and reliability of the leaching methods were described in detail in Wu et al. (2020). In brief, splits of sediment powders were leached with 3 N HNO_3 for 12–16 hours at room temperature and then centrifuged. The supernatant was collected, dried, and further processed with several high-purity acid treatments (aqua regia, conc. HNO_3) in order to decompose any potential organic matter. All the samples (bulk and leaching portions) were finally dissolved in 1 mL of 0.8 M HNO_3 for ion-exchange chromatography.

3.2. V isotopic measurement

The chemical procedure for purification of V and isotopic measurement is described in Wu et al. (2020). In brief, V was purified with a four-step ion exchange procedure by coupling cation- and anion-exchange columns. The cation resin AG50W-X12 (200–400 mesh) was used to remove some major matrix elements (e.g. Fe, Ti, Al, Ca, and Mn). Then AG1-X8 (200–400 mesh) chloride-form anion resin was used to further remove residual matrix and isobaric elements (e.g., K, Na, Mg, and Cr). In between each column, samples were boiled in aqua regia overnight at

Table 1
TAG metalliferous sediment sample data.

	Latitude	Longitude	Sediment depth cm bsf	$\delta^{51}V_{bulk}$ ‰	2SD	n	Al wt.%	Ca wt.%	Fe wt.%	Mn wt.%	Ti wt.%	V µg/g
Sediments off the active TAG mound												
MAR-C3	26°09.40′N	44°49.00′W	0–1	−0.15	0.03	2	0.98	25.6	11.33	0.13	0.08	270
AMKG1895 grab	26°08.50′N	44°48.45′W	0–15	−0.41	0.06	2	1.27	20.1	2.58	1.01	0.08	71
AMKG1891	26°09.05′N	44°48.70′W	0–1	−0.35	0.01	3	1.02	30.9	4.68	0.97	0.08	139
AMKG1810	26°08.29′N	44°48.65′W	0–1	−0.28	0.11	2	1.74	45.0	3.20	0.14	0.12	84
AMKG1825	26°10.38′N	44°47.70′W	0–2	−0.34	0.04	2	1.19	34.0	1.85	0.13	0.08	58
AMKG1820	26°08.72′N	44°48.45′W	0–1	−0.21	0.04	3	1.13	30.6	4.24	0.14	0.09	130
AMKG1893	26°09.10′N	44°49.35′W	0–2	−0.35	0.06	2	1.01	28.9	1.65	0.09	0.07	59
AMKG1799	26°08.10′N	44°49.70′W	0–1	−0.28	0.04	2	1.82	32.7	4.15	0.12	0.13	96
CD102/43/1	26°09.26′N	44°48.90′W	0–5	−0.21	0.11	3	0.69	20.6	14.24	0.40	0.07	289
CD102/18/1	26°08.53′N	44°48.38′W	0–5	−0.31	0.06	3	0.77	27.9	7.95	0.49	0.07	202
CD102/53A	26°09.26′N	44°48.93′W	0–5	−0.28	0.05	3	0.90	28.1	8.35	0.18	0.08	190
CD102/19	26°08.59′N	44°48.22′W	0–5	−0.24	0.07	3	1.02	30.3	6.08	0.35	0.09	181
Sediments on the active TAG mound												
ALV2584	26°08.29′N	44°49.70′W	0–1	−0.35	0.10	2	1.25	34.2	8.81	0.31	0.10	125
			6–7	−0.10	0.06	3	0.09	1.3	34.34	4.13	0.05	215
			14–15	−0.34	0.11	3	0.03	0.3	34.95	0.34	0.01	55
ALV2594	26°08.30′N	44°49.60′W	0–1	−0.14	0.07	3	0.92	0.9	31.41	2.85	0.07	822
			3–4	−0.26	0.06	3	0.45	0.1	20.39	8.92	0.05	385
			8–9	−0.13	0.10	3	0.11	0.1	23.99	6.45	0.02	286
ALV2187 Marker 1986-1	26°08.30′N	44°49.60′W	0–1	−0.03	0.10	4	0.04	1.5	29.03	4.07	0.00	524

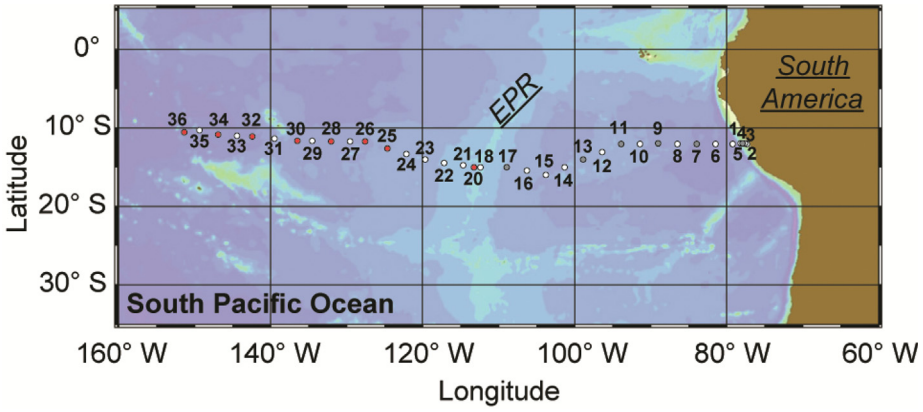

Fig. 3. Station map along the US GEOTRACES Eastern Pacific Zonal Transect (GEOTRACES cruise GP16). The red dots denote the locations of the core-top sediments that were analyzed in this study. The grey dots denote the locations of the core-top sediments that have been studied in Wu et al. (2020).

135 °C to remove potential organic material leached from the resin, evaporated again, and redissolved in the next solution. The yield of the V after purification is 95 ± 5%, with $^{53}Cr/^{51}V$ and $^{49}Cr/^{51}V$ lower than 3×10^{-5}. Purified samples were dissolved in 1 mL 2% HNO_3 prior to elemental and isotopic analysis. The total procedural blank was less than 1 ng, which was negligible compared with the loaded amount of V (2–8 µg).

Vanadium isotopic ratios were measured on Thermo Neptune MC-ICPMS at Woods Hole Oceanographic Institution (WHOI) within the Non-traditional Isotope Research on Various Advanced Novel Applications (NIRVANA) laboratory and at Florida State University (FSU) within the geochemistry group at the National High Magnetic Field Laboratory (NHMFL). Measurements were performed at medium-resolution mode (resolution ΔM/M > 4000) to separate the isotopes of target elements from isobaric interfering molecular species such as $^{36}Ar^{14}N^+$, $^{36}Ar^{16}O^+$, and $^{38}Ar^{14}N^+$ (Nielsen et al., 2016; Wu et al., 2016). Solutions were introduced with desolvating nebulizer system (Aridus II) and Jet sample + X-skimmer cone combination, with a typical sensitivity of ^{51}V of ~1.5–2.5nA/ppm. An amplifier connected with 10^{10} Ω resistor was used to monitor the signal on mass 51, while mass 50 was monitored with a conventional 10^{11} Ω resistor to accommodate the large natural isotope abundance differences of V ($^{51}V/^{50}V \sim 400$). The masses 49 for ^{49}Ti and 53 for ^{53}Cr were simultaneously measured to accurately correct any

potential interferences of ^{50}Ti and ^{50}Cr on ^{50}V (Nielsen et al., 2011; Wu et al., 2016). Sample-standard bracketing method was applied to calibrate instrument mass discrimination effects, using aliquots of the Alfa Aesar (AA) Oxford V standard solution (Nielsen et al., 2011; Prytulak et al., 2011) as the bracketing solution.Vanadium isotopic data are reported in conventional delta notation relative to the AA Oxford V standard ($\delta^{51}V = (((^{51}V/^{50}V)_{sample}/(^{51}V/^{50}V)_{AA} - 1) \times 1000$ (‰)). The in-house solution BDH standard was applied to monitor the stability of the analysis on the MC-ICP-MS, which has been measured in several labs with $\delta^{51}V$ value of −1.2‰ (Nielsen et al., 2011; Schuth et al., 2017; Wu et al., 2016, 2020). Above procedure returns 2SD uncertainties of ±0.12‰, which is based on the long-term external 2SD reproducibility assessed based on replicate measurements of in-house standard solution and USGS reference materials (Nielsen et al., 2019; Wu et al., 2020).

4. RESULTS

The $\delta^{51}V$ data for the metalliferous sediments from the TAG hydrothermal field are presented in Table 1. The bulk $\delta^{51}V$ values of these samples range from −0.41‰ to −0.03‰. These samples have large V concentration variations from 55 μg/g to 822 μg/g, with V/Al ratios ranging from 0.005 to 1.26, much higher than that of average upper continental crust (0.0012, Rudnick and Gao, 2003), Pacific pelagic clay (0.0013, Bischoff et al., 1979), and pelagic sediments that were previously investigated for V isotope compositions by Wu et al. (2020) (0.0031).

The $\delta^{51}V$ data for the EPZT GP16 sediment transect at the west of SEPR are presented in Table 2. The data for EPZT GP16 sediments to the east of SEPR (Wu et al., 2020) are also presented in Table 2 for comparison. The bulk $\delta^{51}V$ values of EPZT GP16 sediments at the west of EPR range from −0.73‰ to −0.52‰, heavier than that of EPZT GP16 sediments collected at the east of EPR (−0.95‰ to −0.80‰). These sediments show V/Al ratios ranging from 0.0016 to 0.1003, which is generally higher than that of the average upper continental crust and Pacific pelagic clays. The leachable fraction of these sediments show $\delta^{51}V_{leach}$ variations from −0.42‰ to −0.03‰, similar to the $\delta^{51}V$ of the TAG hydrothermal sediments, while much heavier than the leachable fractions of the EPZT GP16 sediments at the east of EPR (−0.98‰ to −0.72‰).

5. DISCUSSION:

5.1. The control of V isotope composition in hydrothermal sediments

The metalliferous sediments from TAG hydrothermal field mainly exhibit bulk $\delta^{51}V$ values ranging from −0.4 to −0.1‰ (Table 1), with strong enrichment of V (V/Al ~ 0.005–1.2) compared to that of average upper continental crust (V/Al = 0.0012, Rudnick and Gao, 2003), implying little or no influence from detrital particles on the measured bulk V isotope compositions. This conclusion is supported by the lack of correlation between V/Al ratio and $\delta^{51}V$. Furthermore, a detrital V correction for the sample (AMKG1825) with the lowest V/Al ratio (assuming $\delta^{51}V = -0.7$‰ for detrital material) only results in a correction of 0.06‰ $\delta^{51}V$-units, which is smaller than the analytical uncertainty. Thus, the $\delta^{51}V$ values of the bulk hydrothermal sediments represent the authigenic signatures likely associated with the V-rich authigenic minerals present in the sediments.

Geochemical studies of hydrothermal particles have shown that V is enriched in Fe oxyhydroxide particles within the hydrothermal plume (Trocine and Trefry, 1988; German et al., 1991; Trefry and Metz, 1989), whereas hydrothermal Fe sulfide particles have been suggested to contain negligible amounts of V (Rudnicki and Elderfield, 1993). Experiments of basalt alteration have also documented very low solubility of V in fluids during seawater alteration of basalt (Seyfried and Mottl, 1982), which is consistent with the unmodified V concentrations observed in basalts altered by high-T fluids (Bach et al., 2003). In addition, previous study has shown that low-temperature hydrothermal fluid have very low V concentrations (Wheat et al., 2002). These works all indicate that the hydrothermal fluid have little amount of V so that could not be the source of V enriched in Fe oxyhydroxide particles. Instead, the uptake of V into particles within the hydrothermal plume occur by scavenging from seawater onto Fe-oxyhydroxide phases that form when vent-derived fluids mix with cold, oxygenated seawater (German et al., 1991; Rudnicki and Elderfield, 1993). Therefore the settling of the hydrothermally derived plume particulates can result in the enrichment of V in hydrothermal metalliferous sediments as we observed in the metalliferous sediments from TAG hydrothermal field.

The concentration of V in the shallow metalliferous sediments off the TAG mound exhibit pronounced linear correlations with Fe ($R^2 = 0.957$, Fig. 4), which also follows the trend shown by previous studies of TAG hydrothermal sediments (Metz et al., 1988). Such linear correlations are similar to those observed in the particulates from neutrally buoyant plumes (e.g. German et al., 1991), which confirms that the accumulation of V in the metalliferous sediments off the TAG mound is controlled by the sedimentation of hydrothermal Fe oxyhydroxides, most likely ferrihydrite and goethite (Toner et al., 2009). It is also notable that the V/Fe ratio in the hydrothermal fraction of the sediment off the TAG mound (0.0026) is significantly lower than that of the plume particulates from the TAG hydrothermal field (0.0044, Trefry and Metz, 1989; German et al., 1991) (Fig. 4). The lower V/Fe ratio of the metalliferous sediment relative to the plume particle value is also observed at the EPR (Schaller et al., 2000), which has been attributed to (1) variation of element incorporation during iron oxide formation as a function of grain size and rate of precipitation; (2) secondary iron oxides formed from V-poor sulfides; and (3) phase transformation of iron oxides leading to the redistribution of V. The metalliferous sediments on the TAG mound contain high abundances of Fe sulfides (Mills et al. 1993), which have been suggested to undergo strong sulfide oxidation and diagenetic phase transformation after deposition (German et al. 1993; Goulding et al.,

Table 2
EPZT GP16 core-top sediment sample data.

	Latitude	Longitude	Bulk data									Leaching data					
			$\delta^{51}V$ ‰	2SD	n	Al wt.%	Ca wt.%	Fe wt.%	Mn wt.%	Ti wt.%	V μg/g	$\delta^{51}V$ ‰	2SD	n	Al wt.%	Ti wt.%	V μg/g
MC36	10°30.02′S	152°00.03′W	−0.71	0.08	3	6.12	1.5	3.66	0.94	0.27	119	−0.03	0.06	2	3.87	0.05	22
MC34	10°45.87′S	147°30.05′W	−0.73	0.04	2	5.68	3.4	5.70	1.32	0.41	92	−0.07	0.05	2	2.89	0.05	23
MC32	11°01.83′S	142°57.01′W	−0.73	0.07	2	7.00	4.8	9.13	0.99	1.68	135	−0.21	0.00	2	1.30	0.06	26
MC30	11°34.83′S	136°58.86′W	−0.71	0.03	2	0.58	29.4	0.79	0.18	0.07	26	−0.42	0.13	2	0.24	0.02	12
MC28	11°37.57′S	132°30.02′W	−0.69	0.02	2	0.14	24.8	0.84	0.23	0.02	24	−0.26	0.01	2	0.21	0.01	14
MC26	11°40.21′S	128°00.00′W	−0.68	0.08	2	0.18	41.2	0.98	0.24	0.01	20	−0.38	0.12	2	0.13	0.01	15
MC25	12°32.53′S	124°59.97′W	−0.54	0.04	2	0.71	37.7	2.89	0.58	0.03	23	−0.37	0.08	2	0.11	0.00	20
MC20	15°00.01′S	113°30.02′W	−0.52	0.03	2	0.14	35.6	5.28	1.26	0.00	137	−0.10	0.12	2	0.05	0.00	88
MC17*	14°59.99′S	109°11.43′W	−0.95	0.06	2	0.20	43.7	0.35	0.16	0.01	5	−0.98	0.05	2	0.08	0.00	5
MC13*	14°00.01′S	99°00.00′W	−0.90	0.03	2	0.38	40.5	0.76	0.34	0.02	12	−0.85	0.01	2	0.15	0.01	9
MC11*	11°59.98′S	94°00.00′W	−0.85	0.13	2	0.27	37.1	0.26	0.11	0.01	5	NA			NA	NA	NA
MC9*	12°00.02′S	89°00.06′W	−0.80	0.07	2	3.87	13.8	3.28	0.68	0.17	94	−0.72	0.11	2	0.72	0.02	22
MC7*	12°00.00′S	84°00.04′W	−0.93	0.08	2	7.15	1.0	4.29	0.53	0.29	165	−0.73	0.03	2	0.77	0.01	31
MC4*	12°02.69′S	77°49.09′W	−0.81	0.01	2	5.20	5.8	2.76	0.03	0.26	120	−0.72	0.05	2	0.32	0.01	20

NA: not analyzed.
* Data from Wu et al. (2020).

1998). Despite their variable V/Fe ratios (Fig. 4) and complex diagenesis, the metalliferous sediments on the TAG mound show generally similar ranges of $\delta^{51}V$ values compared to those off the TAG mound (Fig. 5), which implies limited V isotope fractionation during diagenetic phase transformation. This conclusion is supported by V isotope data for diagentically modified continental margin sediments that were also associated with negligible V isotope modification under both oxic and anoxic conditions (Wu et al., 2020). Thus, the V isotope composition in the metalliferous sediments is most likely inherited and minimally altered, if at all, from the oxyhydroxide minerals that formed in the hydrothermal plume, rather than overprinted by secondary post-depositional processes.

Based on the above discussion, it is reasonable to speculate that the V isotope composition of hydrothermal metalliferous sediments is controlled by the isotope fractionation during the incorporation of V from seawater into Fe-Mn oxyhydroxide phases, which has also been suggested to control the V isotope composition of marine hydrogenetic ferromanganese crusts (Wu et al., 2019a, 2019b) and oxic sediments (Wu et al., 2020). However, the metalliferous sediments from TAG hydrothermal field exhibit significantly higher $\delta^{51}V$ values (−0.4 to −0.1‰) compared to those of marine hydrogenetic ferromanganese crusts (-1.0 ± 0.2‰, Wu et al., 2019a, 2019b) and oxic sediments (-0.9 ± 0.3‰, Wu et al., 2020). The observed V isotope variations among these sediments might be related to changes in isotope fractionation during the uptake of V from seawater within the hydrothermal plume, and mineralogical differences between oxic deep-sea sediments and those precipitating from hydrothermal plume particulates.

The TAG sediments off the mound show a slightly negative correlation between $\delta^{51}V$ and Mn/Fe ratios (Fig. 5), which implies that Fe and Mn-rich oxide minerals in these sediments could have distinct V isotope compositions that influence the V isotope composition of these sediments. Here simple mixing lines are constructed, which indicates that although the V isotope composition of hydrothermal sediment is mainly controlled by Fe oxide minerals, Mn oxide minerals may also contribute. It is, however, notable that the mixing line that fits the hydrothermal sediment and Fe-Mn crust data best (line labeled 0.2 in Fig. 5), uses $\delta^{51}V = -3$‰ for the Mn oxide endmember, which is far lighter than any terrestrial material measured to date and unlikely to reflect Mn oxides in Fe-Mn crusts (Wu et al 2020). It is, thus, unclear whether Mn oxides account for a significant portion of V in some hydrothermal sediments. Different fractionation factors have been observed for the adsorption of metals like Mo (Barling and Anbar, 2004; Goldberg et al, 2009) and Zn (Pokrovsky et al., 2005) onto different Fe and Mn oxyhydroxides phases. Thus, V isotope fractionation could also vary during adsorption onto different Fe and Mn oxyhydroxides phases. At present, exact V isotope fractionation factors during adsorption of V onto various Fe and Mn oxyhydroxide phases remain unknown. Therefore, further experimental work is required to test this hypothesis.

It is also notable in the diagram of Mn/Fe ratio vs $\delta^{51}V$ value (Fig. 5) that the hydrothermal sediments and pelagic

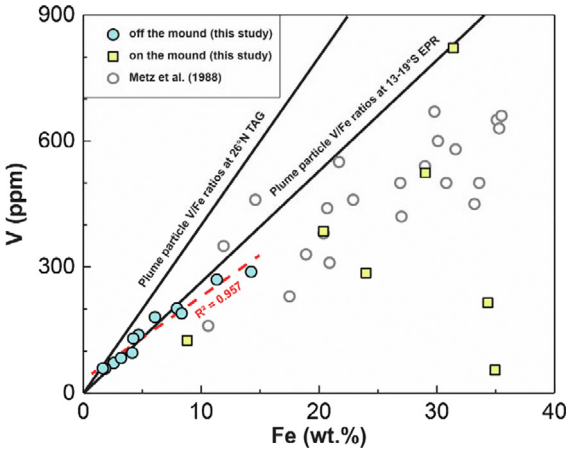

Fig. 4. The content of V (ppm) versus Fe (wt.%) in the studied metalliferous sediments in TAG hydrothermal field. The data of 26°N TAG hydrothermal sediments from Metz et al. (1988) without sulfide minerals and secondary iron oxides are also plotted. The black lines are defined by the V/Fe ratios of plume particle from TAG hydrothermal field (German et al., 1991) and 13–19°S EPR hydrothermal field (Feely et al., 1996).

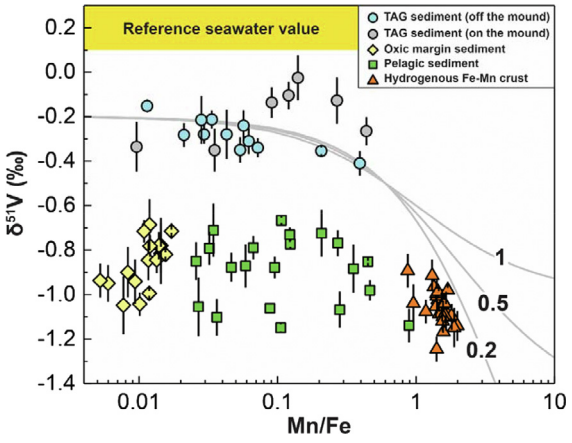

Fig. 5. $\delta^{51}V$ versus Mn/Fe ratio of TAG hydrothermal sediments compared with non-hydrothermal oxic sediments from the literature. $\delta^{51}V$ of oxic margin sediment (yellow diamond) and pelagic sediment (green square) are from Wu et al. (2020); $\delta^{51}V$ of hydrogenous Fe-Mn crust (orange triangle) are from Wu et al. (2019a); reference seawater $\delta^{51}V$ is from Wu et al. (2019b). Mixing lines between Fe oxide endmember and Mn oxide endmember are shown with solid lines. The number in each line shows the ratios of V concentration between that in the Mn oxide mineral endmember ($[V]_{Mn\text{-}oxide}$) and Fe oxide mineral endmember ($[V]_{Fe\text{-}oxide}$). Considering the good V-Fe correlation in hydrothermal sediments off the mound, $[V]_{Mn\text{-}oxide}/[V]_{Fe\text{-}oxide}$ should be less than one. The $\delta^{51}V$ of Fe oxide mineral endmember is set at −0.2‰ from the $\delta^{51}V$ of hydrothermal sediments with the lowest Mn/Fe ratio. The $\delta^{51}V$ of Mn oxide mineral endmember is set to mimic the observed trend for TAG sediments off the mound, i.e. −1‰, −1.5‰, and −3‰ when $[V]_{Mn\text{-}oxide}/[V]_{Fe\text{-}oxide}$ is 1, 0.5, 0.2, respectively.

sediments have a similar range of Mn/Fe ratios despite their different $\delta^{51}V$ variations. Thus, the difference of $\delta^{51}V$ between hydrothermal sediments and non-hydrothermal oxic sediments could not solely be ascribed to the different mineralogy of Fe and Mn oxyhydroxides in these sediments. Previous observations have shown increasing V/Fe ratios within buoyant hydrothermal plumes (Feely et al., 1991; German et al., 1991). For comparison, the Fe oxyhydroxide particulates in neutrally buoyant portions of the hydrothermal plume exhibit fixed V/Fe ratios, which do not vary significantly with dilution or downstream dispersal distance (Trefry and Metz, 1989; German et al., 1991; Feely et al., 1996, 1998; Edmonds and German, 2004). These studies indicate that V undergoes rapid scavenging from seawater at the time of, or soon after, the precipitation of Fe oxyhydroxide during buoyant plume rise, and no further exchange of V with seawater occurs as the particles are dispersed away from the vent source within the neutrally buoyant plume. Such a conclusion is also supported by field and laboratory experiments (Metz and Trefry, 1993). Thus the accumulation of V in hydrothermal particles occurs at the early stage of seawater-hydrothermal fluid mixing along with particulate Fe-oxyhydroxide formation, which might control the V isotope fractionation behavior.

As discussed above, the scavenging of V occurs rapidly at the initial stage of seawater-hydrothermal fluid mixing along with particulate Fe-oxyhydroxide formation within buoyant hydrothermal plumes. Hydrothermal fluids have solution chemistry distinctly different than seawater (e.g. low pH and/or high H_2S content, e.g. Mottl et al., 2011; Wheat et al., 2002). Thus, there might be some transient difference in either the characteristics of the Fe-oxyhydroxides that the V binds to and/or the speciation of the V within these turbulent plumes compared to that of the modern oxic ocean. Experimental studies using other metal isotopes have shown that isotope fractionation during metal adsorption onto oxyhydroxides could vary with variations in solution chemistry like pH (e.g. Pokrovsky et al., 2005; Goldberg et al., 2009) and ionic strength (e.g. Wasylenki et al., 2014; Bryan et al., 2015). This might also be the case for V, as the species of V and the coordination structure of adsorbed V at the oxyhydroxide surface could vary with solution pH (e.g. Peacock and Sherman, 2004), which might induce changes in V isotope fractionation factors during V adsorption (Wu et al., 2015) but needs to be tested with future work. In addition, considering the presence of dissolved hydrogen sulfide and polymetallic sulfide phases in some buoyant plumes (e.g. Radford-Knoery et al., 2001), reduced V species (like vanadyl) might form before being incorporated by Fe-oxyhydroxide.

On the other hand, a chemical model developed by Rudnicki and Elderfield (1993) suggests that more than 67% of V is removed from the seawater by coprecipitation during oxyhydroxide particle formation. The removal of V, in this case, could be regarded as a (semi-)closed process and, thus, the formed particulates would have V isotope compositions closer to the seawater value as compared with the fractionation factors observed for the authigenic component in open ocean oxic sediments (e.g. Rolison et al., 2017; Wu et al., 2020). Kinetic isotope fractionation where the light V isotope is preferentially incorporated during the rapid Fe-oxyhydroxide precipitation could also explain the observed values. Previous experimental study showed that

the extent of Mg isotope fractionation decreases with the increase of calcite precipitation rate (Mavromatis et al., 2013). This is thought to reflect the kinetic effects related to mineral growth rate, which could be explained in the control of transport and surface reaction during crystal growth (DePaolo, 2011). Experimental study also showed that the isotopic fractionation of Cd into calcite is modulated by the rate of Cd uptake during growth of calcite, with faster uptake of Cd leads to quantitative uptake of Cd and thus minimal isotope fractionation (Horner et al., 2011). Thus, kinetic isotope fractionation due to the fast uptake of V during the rapid Fe-oxyhydroxide precipitation could also explain the observed values. However, currently it is not possible to directly discern kinetic from equilibrium effects for V isotopes based on our TAG sediment data. Further particulate observations and, in particular, experimental studies are required to better constrain the underlying mechanisms controlling V isotope compositions in hydrothermal sediments. Despite these uncertainties, our data set shows that modern hydrothermal metalliferous sediments exhibit systematically different V isotope compositions compared to those observed for non-hydrothermal oxic sediments.

5.2. Persistence of V during long-range transport of hydrothermal particles

The GP16 sediments collected to the west of SEPR, show slight to high enrichment of V compared to the average upper continental crust (Rudnick and Gao, 2003), with V EF (enrichment factor, V EF = $(V/Al)_{sample}/(V/Al)_{UCC}$) from 1.2 to 84.3 (Fig. 6A). Therein, there is strong evidence of both V and Fe accumulation in the GP16 sediments collected between 113°W and 137°W longitude, as they have elevated Fe/Al ratios (1.4–38.7) relative to average upper continental crust (0.48, Rudnick and Gao, 2003). Previous studies have demonstrated the long-range western lateral transport of dissolved and particulate iron and manganese from the SEPR hydrothermal field (Resing et al., 2015; Fitzsimmons et al., 2017). Thus, the elemental systematics of these sediments suggest that hydrothermal particles not only are transported across the Pacific ocean, they also appear to have a substantial impact on the elemental budgets of the GP16 sediments. It is known that the GP16 section underlies the oligotrophic part of the ocean in the central Pacific with low settling fluxes of both detrital and biogenic particulate. For this reason, it is easy for hydrothermal signatures to go undiluted here compared to most other ridge sections.

In terms of V isotopes, we use only the leachable fractions as the best representation of the authigenic V in the GP16 sediments, which is in accordance with the relatively significant detrital V components in these types of sediments and the efficacy of the employed leaching method (Wu et al., 2020). Despite their various extents of V enrichment as discussed above, sediments to the west of SEPR all exhibit heavier compositions compared to those to the east of SEPR and other non-hydrothermal oxic sediments (Wu et al., 2020) (Fig. 6B). Furthermore, samples to the west of SEPR where hydrothermal particles have been detected in the water column (Resing et al., 2015; Fitzsimmons et al 2017) display V isotope compositions identical to those observed for the metalliferous sediments from TAG hydrothermal field (Fig. 6B). These observations are independent of the proportion of leachable V in the sediment both east and west of the SEPR (Fig. 6A), which demonstrates that the leaching method cannot explain the isotopic differences observed. Based on these arguments, we conclude that the GP16 sediments to the west of SEPR have accumulated significant authigenic V from hydrothermal particulates that settled out of the water column following predictions made based on particulate and dissolved Fe and Mn data from the water column above (Fitzsimmons et al., 2017). Our findings thus document that hydrothermal particles also transport V exceptionally large distances in the ocean.

Previous observations showed that the particulate Fe across the plume at the GP16 section have invariable Fe isotope compositions, indicating that hydrothermally sourced particulate Fe speciation is preserved without further fractionating transformations during plume advection (Fitzsimmons et al., 2017). Our results similarly imply that the hydrothermal particulates preserve the original V isotope composition they obtained during initial V adsorption to or co-precipitation with Fe oxyhydroxide even after long-range transport away from the hydrothermal source. This observation implies that further scavaging or exchange of V between seawater and particulates during transport is minimal. Such a conclusion is consistent with results from previous laboratory experiments (Metz and Trefry, 1993) as well as measurements of particulates in hydrothermal plumes that exhibited fixed V/Fe ratios as a function of dilution with seawater and downstream dispersal distance (Trefry and Metz, 1989; German et al., 1991; Feely et al., 1996, 1998; Edmonds and German, 2004). In addition, previous work showed that the form of hydrothermal particulate Fe at GP16 section exhibit a marked morphological transition from Fe(III) oxyhydroxides aggregates to discrete Fe(III) oxyhydroxide minerals embedded within a matrix of organic carbon beyond ~100–200 km off-axis at SEPR (Fitzsimmons et al., 2017). The covering of discrete Fe(III) oxyhydroxide with organic carbon might hinder further V isotopic exchange between the particles and surrounding seawater.

Although V behaves conservatively with respect to Fe within all known neutrally buoyant hydrothermal plumes, the V/Fe ratios in hydrothermal plume particulates vary between different hydrothermal fields, despite the relatively invariant V content of ambient seawater (Trefry and Metz, 1989; Feely et al., 1992, 1994, 1996, 1998; Edmonds and German, 2004). It has been suggested that coprecipitation of phosphorous and Fe may influence V incorporation in hydrothermal particles (Feely et al., 1998; Edmonds and German, 2004), although corresponding sediments do not show such a relationship. Our results show that the sediments from TAG hydrothermal field and close to SEPR hydrothermal field have $\delta^{51}V$ values within the range of each other. Thus, regardless of whether this process is important or not for V abundances in hydrothermal sediments, it does not appear to affect V isotope fractionation

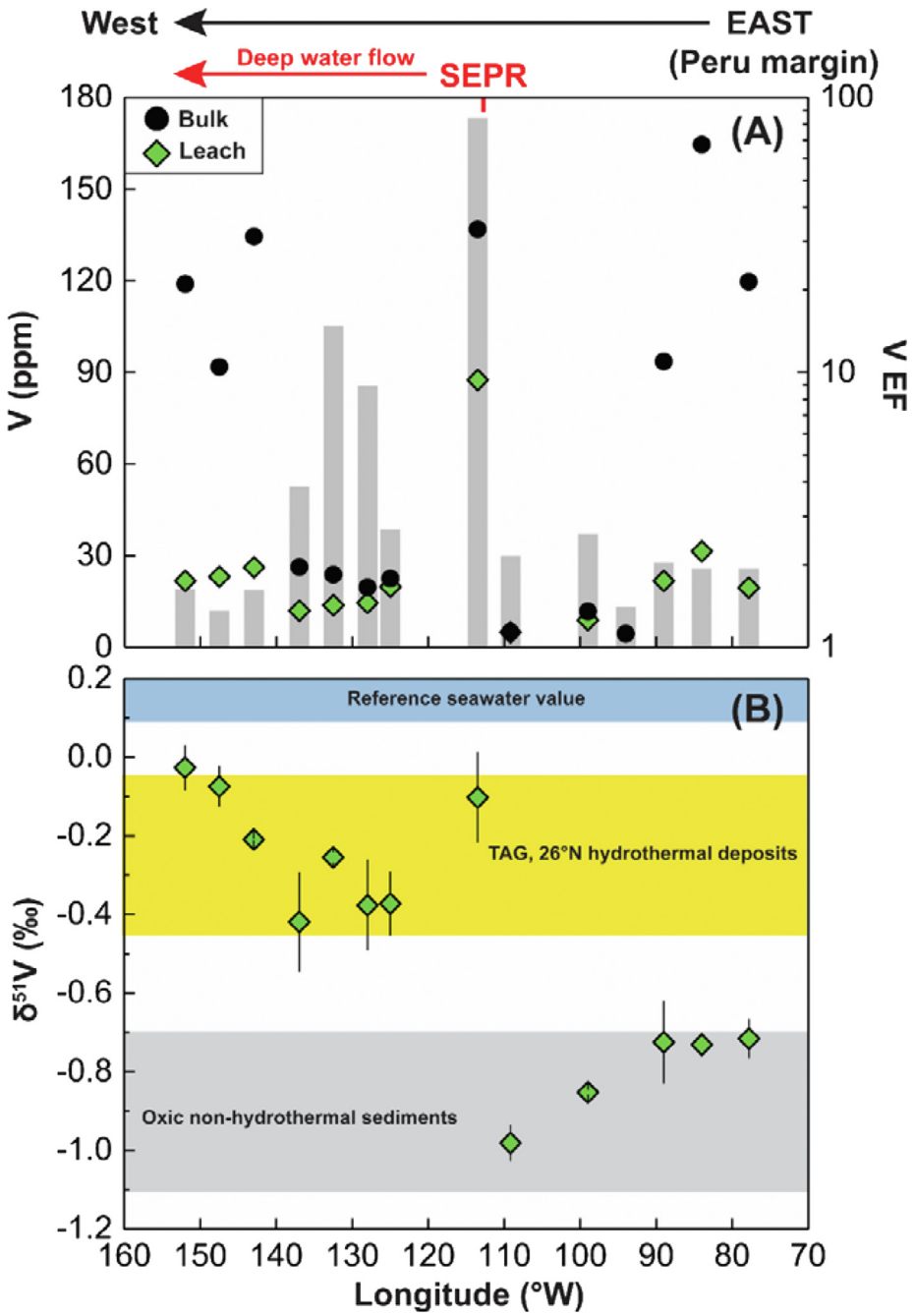

Fig. 6. Spatial distribution of (A) bulk (black circles) and leach (green diamonds) V contents and bulk enriched factors (EF) (grey bars), and (B) leach $\delta^{51}V$ values for the studied core-top sediments along the GEOTRACES EPZT GP16 cruise using the same symbols. Grey bar in (A) denotes the V EF of the sediments. The yellow area in (B) shows the $\delta^{51}V$ range of metalliferous sediments in TAG hydrothermal field. The grey area in (B) shows the previously published $\delta^{51}V$ range of oxic non-hydrothermal sediments (Wu et al., 2020). The data of EPZT sediments at the east of SEPR are from Wu et al. (2020).

between seawater and hydrothermal sediments. Further V isotope work on sediments from other hydrothermal fields is required to test this assumption. Regardless, we conclude that the average $\delta^{51}V$ value of all our hydrothermal sediments (-0.2 ± 0.1‰, 2SE) represents the current best estimation for the V isotope composition of modern marine hydrothermal sediments.

5.3. Implications on the marine isotopic budget of V

In the modern ocean, hydrothermal sediments are known to constitute a significant marine V sink as it is scavenged onto hydrothermal particulates (Trefry and Metz, 1989). However, current estimates of the hydrothermal V flux show a wide range of values, ranging from about

10% to more than 70% of the riverine influx of V (Trefry and Metz, 1989; Rudnicki and Elderfield,1993; Morford and Emerson, 1999; Nielsen, 2021). All these previous studies estimate the hydrothermal V flux by multiplying the average V/Fe ratios in hydrothermal particulates with the hydrothermal Fe precipitation flux. However, as discussed above, there is a clear difference between V/Fe ratios in particulates and corresponding metalliferous sediments (Fig. 4 and Table 3). Considering that the hydrothermal V sink is exclusively represented by burial in sediments, it seems to be more robust to estimate the hydrothermal V output flux using the sedimentary V/Fe ratios rather than particulate V/Fe ratios.

Thus, the hydrothermal V flux is re-evaluated here. The hydrothermal output flux of V (J_{HT}) can be calculated with the following equation:

$$J_{HT} = HT_{FluidFlux} \times Fe_{HT-fluid} \times f_{Fe-ox} \times (V/Fe)_{HT-seds} \quad (1)$$

where $HT_{FluidFlux}$ is the total volume of high-temperature hydrothermal fluid fluxes, $Fe_{HT\text{-}fluid}$ is the average Fe concentration of endmember hydrothermal fluids, $f_{Fe\text{-}ox}$ is the proportion of hydrothermal Fe precipitated as Fe oxyhydroxides, and $(V/Fe)_{HT\text{-}seds}$ is the average V/Fe ratios of the authigenic component in hydrothermal sediments.

The high-temperature hydrothermal fluid flux ($HT_{FluidFlux}$) has been comprehensively estimated by two studies with independent methods, which reveal similar results of $8 \pm 2 \times 10^{12}$ kg/yr (Coogan and Dosso, 2012; Nielsen et al., 2006). The average Fe concentration of endmember hydrothermal fluids ($HT_{FluidFlux}$) is estimated to be ~4 ± 0.5 mmol/kg based on the recently published MARHYS database that has compiled all the endmember hydrothermal fluid data published to date (Table 3) (Diehl and Bach, 2020). As the buoyant plume evolves, both Fe-sulfide and Fe-oxyhydroxides are precipitated. With the application of an in-situ filtration method, Waeles et al. (2017) showed that no more than 10% of hydrothermal Fe is precipitated as sulfide after being exported with the vent fluid. Previous Fe isotope studies on hydrothermal plume systems also indicate that ~0 to 25% of Fe is lost during buoyant plume rise as Fe sulfide precipitates (Severmann et al., 2004; Bennett et al., 2009). In addition, about 0.33% to up to 4% of the total Fe emitted from hydrothermal vent fields are thought to be stabilized against precipitation from solution due to the presence of organic Fe complexes and Fe colloids (Bennett et al., 2009; Sander and Koschinsky, 2011). Based on these studies, the proportion of hydrothermal Fe precipitated as Fe oxyhydroxides ($Fe_{HT\text{-}fluid}$) is estimated to be 85 ± 5%. The molar $(V/Fe)_{HT\text{-}seds}$ ratio is estimated to be ~0.003 ± 0.001 based on the compiled authigenic V/Fe ratios in hydrothermal sediments (Table 3). Thus, the hydrothermal V output flux (J_{HT}) is estimated to be 82 ± 35 Mmol/yr, if we implement the parameters estimated above.

We further apply the widely-used balance model modified after Richter et al (1992), to assess the effect of V removal by hydrothermal precipitation on the marine cycle of V and provide constraints on the modern marine hydrothermal V flux. In this model, the oceanic elemental and isotopic budget of V are defined by the following equations:

$$dN/dt = \Sigma J_{input} - \Sigma J_{output} \quad (2)$$

$$d(N \times \delta_{sw})/dt = \Sigma(\delta_{input} \times J_{input}) - \Sigma((\Delta_{output} + \delta_{SW}) \times J_{output}) \quad (3)$$

where N is the total number of moles of V in seawater, δ_{sw} and δ_{input} are the $\delta^{51}V$ values for seawater and global inputs, respectively, J_{input} and J_{output} are the input and output fluxes, and Δ_{output} is the fractionation offset of the $\delta^{51}V$ value between the seawater and each output flux.

The open ocean seawater is thought to have homogeneous V isotope composition with $\delta^{51}V = +0.2 \pm 0.1‰$ (2SE) (Wu et al., 2019a). Rivers constitute a major input of V to the ocean, with the estimated isotopic composition of $\delta^{51}V = -0.6 \pm 0.1‰$ (2SE) based on a recent V isotope study on river water (Schuth et al., 2019). The main sinks of V in the modern ocean are oxic sediments, anoxic sediments, euxinic sediments, and hydrothermal sediments (Morford and Emerson, 1999; Nielsen, 2021). Oxic sediments likely accumulate V through adsorption onto Fe-Mn (oxyhydr)oxides, with an estimated value for the authigenic component of $\delta^{51}V = -0.9 \pm 0.1‰$ (2SE) based on recent V isotope study of pelagic sediments, oxic continental margin sediments, and Fe-Mn crusts (Wu et al., 2019b, 2020). In reducing seawater, pentavalent V species (vanadate) tend to be reduced to tetravalent V species (vanadyl), which could strongly bond with particulate organic matter and thus accumulate into anoxic (defined as sediments deposited under oxygen-deficient water column) and euxinic (defined as sediments deposited under a sulfidic water column) sediments (e.g. Calvert et al., 2015; Ohnemus et al., 2017). The V isotope composition of the authigenic component in anoxic sediments is estimated to be $\delta^{51}V = -0.5 \pm 0.1‰$ (2SE), based on the average value for the anoxic sediments from Peru Margin and Santa Barbara Basin (Wu et al., 2020). The authigenic component in the euxinic Cariaco Basin sediments exhibits $\delta^{51}V = -0.2 \pm 0.1‰$ (2SE) (Wu et al., 2020), which is applied to represent the V isotope composition of the euxinic sink. The $\delta^{51}V$ value of hydrothermal output is estimated to be $-0.2 \pm 0.1‰$ (2SE) as discussed above. Thus the isotope fractionation factors between each sink and seawater are $\Delta_{oxic} = -1.1‰$, $\Delta_{anoxic} = -0.7‰$, $\Delta_{euxinic} = -0.4‰$ and $\Delta_{HT} = -0.4‰$.

Assuming steady state is achieved, the influx of V should be equal to the outflux, i.e. $J_{river} = J_{oxic} + J_{anoxic} + J_{euxinic} + J_{HT}$. Thus, the $\delta^{51}V$ value of seawater is determined by the following equation:

$$\delta_{SW} = \delta_{river} - (\Delta_{oxic} \times f_{oxic} + \Delta_{anoxic} \times f_{anoxic} + \Delta_{euxinic} \times f_{euxinic} + \Delta_{HT} \times f_{HT}) \quad (4)$$

where $f_i = J_i/\Sigma J_{output}$, represents the fraction of V removed by sink 'i'.

Previous works on the estimation of the output flux of V into modern oxic sediments give close results of 430 Mmol/yr (Morford and Emerson, 1999) and 377 Mmol/yr (Nielsen, 2021), even though these fluxes are based on very limited data and are highly uncertain. With the compilation

Table 3
Compilation of Fe and V in hydrothermal system.

		Plume particle		Metalliferous sediment		Endmember vent fluid
		Molar V/Fe	Reference	Molar V/Fe	Reference	Dissoved Fe (mmol/kg)*
Pacific ridge	SEPR, 13-19°S	0.0029	Feely et al. (1996)			3.962
	SEPR, 10°S			0.0024	Schaller et al. (2000)	
	SEPR, 15°S			0.0036	Mills et al. (2010)	
	NEPR, 9-11°30'N	0.0029	Feely et al. (1994)			
	JdFR, Cleft Segment	0.0026	Feely et al. (1998)	0.0032	German et al. (1997)	
	JdFR, Endeavour Segment	0.0028	Feely et al. (1998)			
	JdFR, EP86A	0.0023	Baker et al. (1989)			
	Gorda Ridge	0.0030	Feely et al. (1998)			
Atlantic ridge	TAG, 26°08'N	0.0044	Trefry and Metz (1989)	0.0026	Our work, Metz et al. (1988)	2.686
	Broken Spur, 29°10'N	0.0045	Ludford et al. (1996)			
	Rainbow, 36°N	0.0043	Edmonds and German (2004)	0.0063	Cave et al. (2002)	
Indian ridge	SEIR			0.0024	Pan et al. (2018); Liao et al. (2018, 2019)	4.981
	CIR, Edmond	0.0029	Sands (2006)			
	CIR, Kairei	0.0021	Sands (2006)			
Back-arc						3.954

* Compilation data from MARHYS database (Diehl and Bach, 2020).

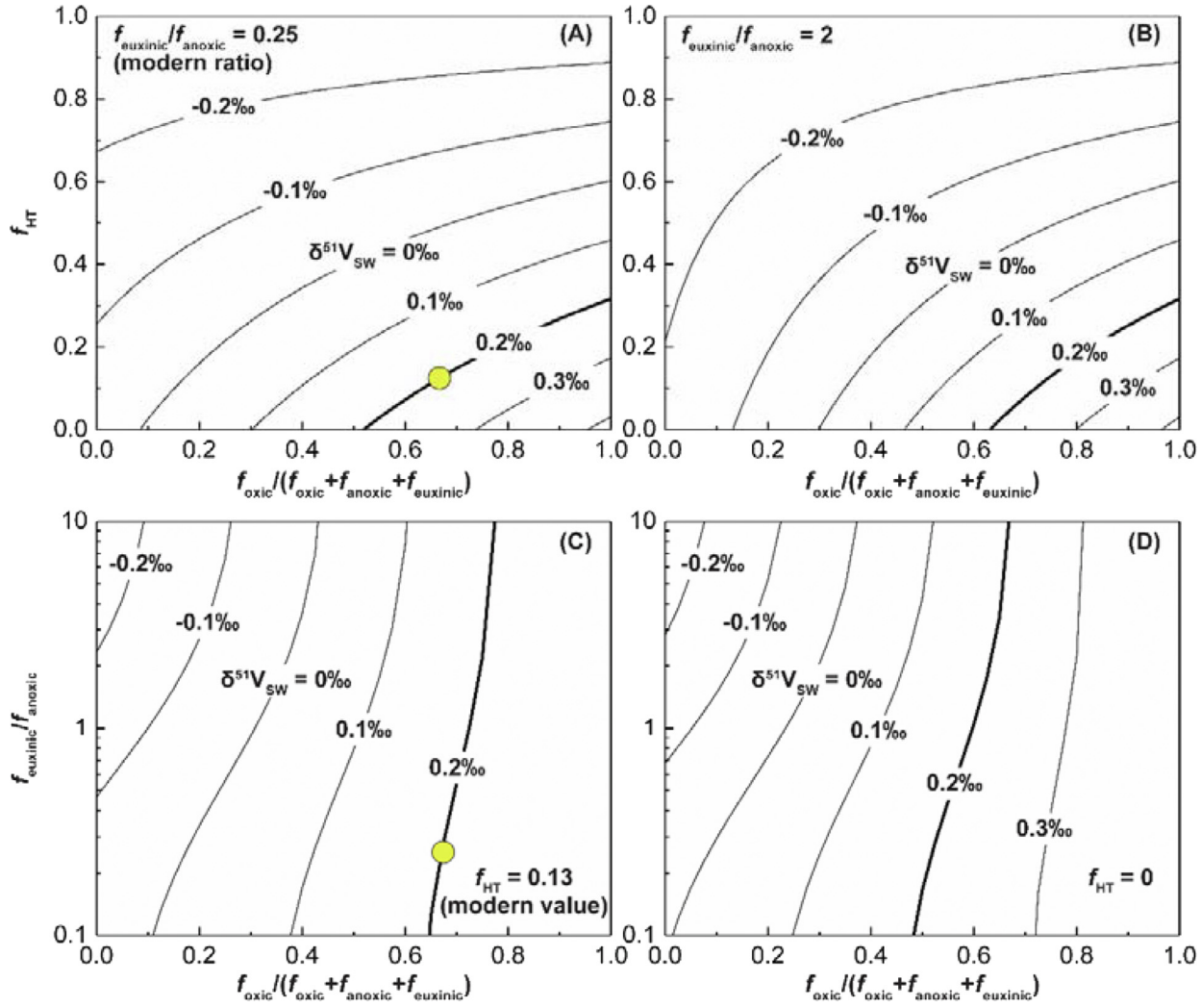

Fig. 7. Mass balance model showing how seawater $\delta^{51}V$ would vary as the relative proportion of V removal (f_{HT}, f_{oxic}, f_{anoxic} and $f_{euxinic}$) changes. The $f_{euxinic}/f_{anoxic}$ ratio is fixed at certain value in (A) $f_{euxinic}/f_{anoxic} = 0.25$, and (B) $f_{euxinic}/f_{anoxic} = 2$, where $f_{euxinic}/f_{anoxic} = 0.25$ is the eatimated present-day value. The f_{HT} value is fixed at certain value in (C) $f_{HT} = 0.13$, and (D) $f_{HT} = 0$, where $f_{HT} = 0.13$ is the eatimated present-day value. The bold line is present-day seawater $\delta^{51}V$ value (+0.2‰, Wu et al., 2019a, 2019b). The yellow dot in (A) and (C) represents the estimated present-day oceanic budget. See model details and the applied parameters are discussed in Section 5.3.

of the core top data of anoxic and euxinic sediments, the average authigenic V fluxes were estimated to be 144 Mmol/yr for anoxic sediments and <39 Mmol/yr euxinic sediments by Nielsen (2021). With our newly estimated hydrothermal output flux (82 Mmol/yr), the fraction of V removed by each sink can be calculated, i.e. f_{oxic} = 59%, f_{anoxic} = 22%, $f_{euxinic}$ = 6%, and f_{HT} = 13%. Combining the output fluxes with the V isotope data, the $\delta^{51}V$ value of the average total output flux is estimated to be $\delta^{51}V \sim -0.68‰$, which is within error of the average riverine input $\delta^{51}V$ value. Thus, despite the relatively large uncertainties on some of the output fluxes, the modern marine V isotope mass balance we construct is at steady state.

The V isotope variations of seawater with the changing of sedimentary output V fluxes could also be evaluated with this model. If the $f_{anoxic}/f_{euxinic}$ ratio is fixed, the changes of δ_{SW} with f_{HT} and the fraction of V flux into oxic sediments relative to the total non-hydrothermal output flux, i.e. $f_{oxic}/(f_{oxic} + f_{anoxic} + f_{euxinic})$ could be developed as shown in Fig. 7A and B. Under persistent oxic deep ocean conditions that prevail in the modern ocean, the flux of V associated with hydrothermal sediments is proportional to the hydrothermal particulate iron fluxes. The marine hydrothermal activity likely varies with the ocean crust production rate, which changes on million-year time scales. Thus, changes in the marine hydrothermal activity could influence the V isotope composition of seawater on long time scales (>Myrs). Substantial changes in the flux of V into anoxic sediments have been suggested based on observations during an oceanic anoxic event (e.g. Owens et al., 2016). During such geologically short-lived climate perturbations events, the variations of $\delta^{51}V$ in seawater would primarily be controlled by the ratio between the reducing and oxic output fluxes. If the f_{HT} is fixed at the modern value,

the changes of δ_{SW} with the relative variations of the reducing and oxic output fluxes would evolve as shown in Fig. 7C. In such a scenario, the global marine $\delta^{51}V$ could vary from 0.2‰ to about −0.1 ‰ with an increased proportion of anoxic sediment V fluxes provided there are no local factors recorded in the sediments.

In an almost entirely reducing and low sulfate ocean, which may have been the case for much of the Precambrian (Canfield, 1998; Lyons et al., 2014), the hydrothermal iron flux is expected to be larger than that in modern time (Kump and Seyfried, 2005). The iron formations deposited in ancient reducing oceans is thought to be influenced by the strong hydrothermal Fe discharge. However, the formation of oxidized iron phases in the prevailing reducing ocean is thought to through photochemical or biologically mediated Fe oxidation (e.g. Planavsky et al., 2010), and/or transformed from mineral precursors like iron-silicate precipitation (Rasmussen et al., 2015) and green rust (Halevy et al., 2017). This contrasts with the particulate Fe-oxyhydroxide formation within hydrothermal plume occurred in the well-oxygenated ocean. Thus, the fluxes of V associated with hydrothermally derived plume particulate seems to be suppressed in the prevailing reducing ocean. If no hydrothermal sink of V ($f_{HT} = 0$) is assumed in this scenario, with modern-like riverine $\delta^{51}V$ values and V isotope fractionation associated with sediments under different redox environments, seawater V isotope composition could change between +0.1‰ and −0.2‰ (Fig. 7D). In addition, the $\delta^{51}V_{SW}$ is more sensitive to the changes of $f_{euxinic}/f_{anoxic}$ ratios when $f_{oxic}/(f_{oxic} + f_{anoxic} + f_{euxinic})$ is low as shown in Fig. 7D. It is also noted that in the modern ocean, the sediments deposited under anoxic and euxinic conditions have similar accumulate rates of V (Piper and Dean, 2002; Nameroff et al., 2004; Scholz et al., 2011). Thus, the changes in $\delta^{51}V$ of seawater would strongly depend on whether anoxic or euxinic conditions, respectively, were the most prevalent in the prevailing reducing ocean. A recent study conducted by Fan et al. (2021) inferred a V isotope composition of seawater of −0.2‰ during the late-Ediacaran, which as shown here (Fig. 7D) and also outlined in Nielsen (2021), implies the predominance of euxinic sediment depositional environments at the time.

As the above models illustrate, the V isotope composition of global seawater could change as a function of the hydrothermal flux on long time scales and the global seawater redox states on long-term and short-term time scales. If the inferred V isotope fractionation factors between different sediment types and seawater have remained constant over time, then it should be possible to utilize a range of different sediment archives (e.g. Fe-Mn crusts, shales, carbonates) to reconstruct the V isotope composition of seawater over time, provided that local sediment depositional environments remained stable. It is also notable that factors other than global redox conditions such as basinal restriction of euxinic marine environments may also influence the sedimentray $\delta^{51}V$ record (Wu et al., 2020). Such local effects might complicate the use of sediments from anoxic/euxinic environments as potential archives for the seawater $\delta^{51}V$ (Nielsen, 2021). Thus, further studies are advocated to further investigate the effects of basinal restriction versus redox on the V isotope compositions in organic-rich sediments. In any case, the V isotope evolution of seawater could provide novel insights into the redox chemistry of the oceans and hydrothermal activity through geologic time.

6. CONCLUSIONS

We present the first vanadium isotope study of the metalliferous sediments from the TAG hydrothermal field and sediments from the Pacific Ocean under influence of the hydrothermal plume arising from SEPR to investigate the processes controlling the V isotope fractionation during the formation of marine sediments related to hydrothermal activity and its influence on the marine isotopic budget of V. The main conclusions are the following:

(1) The hydrothermal sediments have $\delta^{51}V$ values ranging from −0.4 to −0.1‰, which is significantly heavier than those observed in non-hydrothermal oxic sediments (−1.2 to −0.7‰, Wu et al., 2019b, 2020). The V isotope composition of hydrothermal sediments is likely controlled by the isotope fractionation during the rapid initial uptake of V from seawater into hydrothermal Fe oxyhydroxide particulates within the buoyant hydrothermal plume.
(2) The V isotope composition of hydrothermal sediments at the TAG field does not depend on the distance of the active hydrothermal mound. The sediments collected from the deep south Pacific Ocean west of the SEPR all have $\delta^{51}V_{leach}$ values within the range observed in the TAG field, despite some of these sediments being located more than 4000 km from the buoyant portion of the SEPR hydrothermal plume. These results indicate limited V exchange between hydrothermal Fe particles and ambient seawater over vast distances in the ocean.
(3) The hydrothermal V flux output from seawater is re-evaluated here, which is estimated to account for ~13% of the total global removal flux of V. The mass balance model of V isotopes is further established to be at steady state. This model also indicates that the V isotope composition of seawater could change with hydrothermal activity as well as the global seawater redox states on different time scales. Thus, V isotopes have the potential to provide new insights into past ocean chemistry variations.

Declaration of Competing Interest

The authors declare that they have no known competing financial interests or personal relationships that could have appeared to influence the work reported in this paper.

ACKNOWLEDGEMENT

We would like to thank G. White for instrumentation troubleshooting at the MagLab. We are grateful to Linqing Huang and Siqi Li for their help on V isotope analyses. The work was

funded by grants from NSF-OCE 1434785 (JDO and SGN), and NASA Exobiology NNX16AJ60 (JDO and SGN) and 80NSSC18K1532 (JDO and FW). JDO also recognizes support froom the Sloan Research Foundation (FG-2020–13552). A portion of the analyses were performed at the National High Magnetic Field Laboratory in Tallahassee, Florida, which is supported by National Science Foundation Cooperative Agreement No. DMR-1644779 and by the State of Florida. We thank Drew D. Syverson and two anonymous reviewers for their thoughtful and thorough reviews of our manuscript. Noah Planavsky is thanked for editorial handling.

APPENDIX A. SUPPLEMENTARY MATERIAL

Supplementary material to this article can be found online at https://doi.org/10.1016/j.gca.2022.05.002.

REFERENCES

Bach W., Peucker-Ehrenbrink B., Hart S. R. and Blusztajn J. S. (2003) Geochemistry of hydrothermally altered oceanic crust: DSDP/ODP Hole 504B–Implications for seawater-crust exchange budgets and Sr-and Pb-isotopic evolution of the mantle. *Geochem. Geophys. Geosyst.* **4**, 8904.

Baker E., Lavelle J., Feely R., Massoth G., Walker S. and Lupton J. (1989) Episodic venting of hydrothermal fluids from the Juan de Fuca Ridge. *J. Geophys. Res. Solid Earth* **94**, 9237–9250.

Barling J. and Anbar A. D. (2004) Molybdenum isotope fractionation during adsorption by manganese oxides. *Earth Planet. Sci. Lett.* **217**, 315–329.

Barrett T., Taylor P. and Lugoqski J. (1987) Metalliferous sediments from DSDP Leg 92: The East Pacific Rise transect. *Geochim. Cosmochim. Acta* **51**, 2241–2253.

Bennett S. A., Rouxel O., Schmidt K., Garbe-Schönberg D., Statham P. J. and German C. R. (2009) Iron isotope fractionation in a buoyant hydrothermal plume, 5 S Mid-Atlantic Ridge. *Geochim. Cosmochim. Acta* **73**, 5619–5634.

Bischoff J. L., Heath G. R. and Leinen M. (1979) *Geochemistry of deep-sea sediments from the Pacific manganese nodule province: DOMES Sites A, B, and C, Marine geology and oceanography of the Pacific manganese nodule province*. Springer, pp. 397–436.

Bryan A. L., Dong S., Wilkes E. B. and Wasylenki L. E. (2015) Zinc isotope fractionation during adsorption onto Mn oxyhydroxide at low and high ionic strength. *Geochim. Cosmochim. Acta* **157**, 182–197.

Calvert S., Piper D., Thunell R. and Astor Y. (2015) Elemental settling and burial fluxes in the Cariaco Basin. *Mar. Chem.* **177**, 607–629.

Canfield D. E. (1998) A new model for Proterozoic ocean chemistry. *Nature* **396**, 450.

Cave R., German C., Thomson J. and Nesbitt R. (2002) Fluxes to sediments underlying the Rainbow hydrothermal plume at 36 14′ N on the Mid-Atlantic Ridge. *Geochim. Cosmochim. Acta* **66**, 1905–1923.

Chen X., Li S., Newby S. M., Lyons T. W., Wu F. and Owens J. D. (2021) Iron and manganese shuttle has no effect on sedimentary thallium and vanadium isotope signatures in Black Sea sediments. *Geochim. Cosmochim. Acta* **317**, 218–233.

Coogan L. A. and Dosso S. (2012) An internally consistent, probabilistic, determination of ridge-axis hydrothermal fluxes from basalt-hosted systems. *Earth Planet. Sci. Lett.* **323–324**, 92–101.

DePaolo D. J. (2011) Surface kinetic model for isotopic and trace element fractionation during precipitation of calcite from aqueous solutions. *Geochim. Cosmochim. Acta* **75**(4), 1039–1056.

Diehl A. and Bach W. (2020) MARHYS (MARine HYdrothermal Solutions) Database: A global compilation of marine hydrothermal vent fluid, end member, and seawater compositions. *Geochem. Geophys. Geosyst.* **21**, e2020GC009385.

Dong L.-H., Wei W., Yu C.-L., Hou Z.-H., Zeng Z., Chen T. and Huang F. (2021) Determination of Vanadium Isotope Compositions in Carbonates Using an Fe Coprecipitation Method and MC-ICP-MS. *Anal. Chem.* **93**(19), 7172–7179.

Edmond J. M., Measures C., McDuff R., Chan L., Collier R., Grant B., Gordon L. and Corliss J. (1979) Ridge crest hydrothermal activity and the balances of the major and minor elements in the ocean: The Galapagos data. *Earth Planet. Sci. Lett.* **46**, 1–18.

Edmonds H. N. and German C. R. (2004) Particle geochemistry in the Rainbow hydrothermal plume, Mid-Atlantic Ridge. *Geochim. Cosmochim. Acta* **68**, 759–772.

Fan H., Ostrander C. M., Auro M., Wen H. and Nielsen S. G. (2021) Vanadium isotope evidence for expansive ocean euxinia during the appearance of early Ediacara biota. *Earth Planet. Sci. Lett.* **567**, 117007.

Feely R., Baker E., Marumo K., Urabe T., Ishibashi J., Gendron J., Lebon G. and Okamura K. (1996) Hydrothermal plume particles and dissolved phosphate over the superfast-spreading southern East Pacific Rise. *Geochim. Cosmochim. Acta* **60**, 2297–2323.

Feely R. A., Massoth G. J., Baker E. T., Lebon G. T. and Geiselman T. L. (1992) Tracking the dispersal of hydrothermal plumes from the Juan de Fuca Ridge using suspended matter compositions. *J. Geophys. Res. Solid Earth* **97**, 3457–3468.

Feely R. A., Massoth G. J., Trefry J. H., Baker E. T., Paulson A. J. and Lebon G. T. (1994) Composition and sedimentation of hydrothermal plume particles from North Cleft segment, Juan de Fuca Ridge. *J. Geophys. Res. Solid Earth* **99**, 4985–5006.

Feely R. A., Trefry J. H., Lebon G. T. and German C. R. (1998) The relationship between P/Fe and V/Fe ratios in hydrothermal precipitates and dissolved phosphate in seawater. *Geophys. Res. Lett.* **25**, 2253–2256.

Feely R. A., Trefry J. H., Massoth G. J. and Metz S. (1991) A comparison of the scavenging of phosphorus and arsenic from seawater by hydrothermal iron oxyhydroxides in the Atlantic and Pacific Oceans. *Deep Sea Res. Part A Oceanogr. Res. Pap.* **38**, 617–623.

Fitzsimmons J. N., John S. G., Marsay C. M., Hoffman C. L., Nicholas S. L., Toner B. M., German C. R. and Sherrell R. M. (2017) Iron persistence in a distal hydrothermal plume supported by dissolved–particulate exchange. *Nat. Geosci.* **10**, 195–201.

German C., Bourles D., Brown E., Hergt J., Colley S., Higgs N., Ludford E., Nelsen T., Feely R. and Raisbeck G. (1997) Hydrothermal scavenging on the Juan de Fuca Ridge: 23OThxs, 10Be, and REEs in ridge-flank sediments. *Geochim. Cosmochim. Acta* **61**, 4067–4078.

German C., Campbell A. and Edmond J. (1991) Hydrothermal scavenging at the Mid-Atlantic Ridge: modification of trace element dissolved fluxes. *Earth Planet. Sci. Lett.* **107**, 101–114.

German C., Higgs N., Thomson J., Mills R., Elderfield H., Blusztajn J., Fleer A. and Bacon M. (1993) A geochemical study of metalliferous sediment from the TAG Hydrothermal Mound, 26° 08′ N, Mid-Atlantic Ridge. *J. Geophys. Res. Solid Earth* **98**, 9683–9692.

Goldberg T., Archer C., Vance D. and Poulton S. W. (2009) Mo isotope fractionation during adsorption to Fe (oxyhydr)oxides. *Geochim. Cosmochim. Acta* **73**, 6502–6516.

Goulding H., Mills R. and Nesbitt R. (1998) Precipitation of hydrothermal sediments on the active TAG mound: implications for ochre formation. *Geol. Soc. Lond. Special Publ.* **148**, 201–216.

Halevy I., Alesker M., Schuster E. M., Popovitz-Biro R. and Feldman Y. (2017) A key role for green rust in the Precambrian oceans and the genesis of iron formations. *Nat. Geosci.* **10**(2), 135–139.

Ho P., Lee J.-M., Heller M. I., Lam P. J. and Shiller A. M. (2018) The distribution of dissolved and particulate Mo and V along the US GEOTRACES East Pacific Zonal Transect (GP16): The roles of oxides and biogenic particles in their distributions in the oxygen deficient zone and the hydrothermal plume. *Mar. Chem.* **201**, 242–255.

Horner T. J., Rickaby R. E. and Henderson G. M. (2011) Isotopic fractionation of cadmium into calcite. *Earth Planet. Sci. Lett.* **312**(1–2), 243–253.

Kump L. R. and Seyfried, Jr, W. E. (2005) Hydrothermal Fe fluxes during the Precambrian: Effect of low oceanic sulfate concentrations and low hydrostatic pressure on the composition of black smokers. *Earth Planet. Sci. Lett.* **235**(3–4), 654–662.

Lewan M. D. and Maynard J. B. (1982) Factors controlling enrichment of vanadium and nickel in the bitumen of organic sedimentary rocks. *Geochim. Cosmochim. Acta* **46**, 2547–2560.

Liao S., Tao C., Dias Á. A., Su X., Yang Z., Ni J., Liang J., Yang W., Liu J. and Li W. (2019) Surface sediment composition and distribution of hydrothermal derived elements at the Duanqiao-1 hydrothermal field, Southwest Indian Ridge. *Mar. Geol.* **416**, 105975.

Liao S., Tao C., Li H., Zhang G., Liang J., Yang W. and Wang Y. (2018) Surface sediment geochemistry and hydrothermal activity indicators in the Dragon Horn area on the Southwest Indian Ridge. *Mar. Geol.* **398**, 22–34.

Ludford E., Palmer M., German C. and Klinkhammer G. P. (1996) The geochemistry of Atlantic hydrothermal particles. *Geophys. Res. Lett.* **23**, 3503–3506.

Lyons T. W., Reinhard C. T. and Planavsky N. J. (2014) The rise of oxygen in Earth's early ocean and atmosphere. *Nature* **506** (7488), 307–315.

Mavromatis V., Gautier Q., Bosc O. and Schott J. (2013) Kinetics of Mg partition and Mg stable isotope fractionation during its incorporation in calcite. *Geochim. Cosmochim. Acta* **114**, 188–203.

Metz S. and Trefry J. H. (1993) Field and laboratory studies of metal uptake and release by hydrothermal precipitates. *J. Geophys. Res. Solid Earth* **98**, 9661–9666.

Metz S., Trefry J. H. and Nelsen T. A. (1988) History and geochemistry of a metalliferous sediment core from the Mid-Atlantic Ridge at 26 N. *Geochim. Cosmochim. Acta* **52**, 2369–2378.

Mills R., Elderfield H. and Thomson J. (1993) A dual origin for the hydrothermal component in a metalliferous sediment core from the Mid-Atlantic Ridge. *J. Geophys. Res. Solid Earth* **98**, 9671–9681.

Mills R. A., Taylor S. L., Pälike H. and Thomson J. (2010) Hydrothermal sediments record changes in deep water oxygen content in the SE Pacific. *Paleoceanography* **25**, PA4226.

Morford J. L. and Emerson S. (1999) The geochemistry of redox sensitive trace metals in sediments. *Geochim. Cosmochim. Acta* **63**, 1735–1750.

Mottl M. J., Seewald J. S., Wheat C. G., Tivey M. K., Michael P. J., Proskurowski G., McCollom T. M., Reeves E., Sharkey J. and You C.-F. (2011) Chemistry of hot springs along the Eastern Lau Spreading Center. *Geochim. Cosmochim. Acta* **75**, 1013–1038.

Nameroff T., Calvert S. and Murray J. (2004) Glacial-interglacial variability in the eastern tropical North Pacific oxygen minimum zone recorded by redox-sensitive trace metals. *Paleoceanography* **19** PA1010.

Nielsen S. G. (2021) *Vanadium Isotopes: A Proxy for Ocean Oxygen Variations*. Cambridge University Press, Cambridge.

Nielsen S. G., Auro M., Righter K., Davis D., Prytulak J., Wu F. and Owens J. D. (2019) Nucleosynthetic vanadium isotope heterogeneity of the early solar system recorded in chondritic meteorites. *Earth Planet. Sci. Lett.* **505**, 131–140.

Nielsen S. G., Owens J. D. and Horner T. J. (2016) Analysis of high-precision vanadium isotope ratios by medium resolution MC-ICP-MS. *J. Anal. At. Spectrom.* **31**, 531–536.

Nielsen S. G., Prytulak J. and Halliday A. N. (2011) Determination of precise and accurate 51V/50V isotope ratios by MC-ICP-MS, part 1: chemical separation of vanadium and mass spectrometric protocols. *Geostand. Geoanal. Res.* **35**, 293–306.

Nielsen S. G., Rehkämper M., Teagle D. A. H., Butterfield D. A., Alt J. C. and Halliday A. N. (2006) Hydrothermal fluid fluxes calculated from the isotopic mass balance of thallium in the ocean crust. *Earth Planet. Sci. Lett.* **251**, 120–133.

Ohnemus D. C., Rauschenberg S., Cutter G. A., Fitzsimmons J. N., Sherrell R. M. and Twining B. S. (2017) Elevated trace metal content of prokaryotic communities associated with marine oxygen deficient zones. *Limnol. Oceanogr.* **62**, 3–25.

Owens J. D., Reinhard C. T., Rohrssen M., Love G. D. and Lyons T. W. (2016) Empirical links between trace metal cycling and marine microbial ecology during a large perturbation to Earth's carbon cycle. *Earth Planet. Sci. Lett.* **449**, 407–417.

Pan A., Yang Q., Zhou H., Ji F., Wang H. and Pancost R. D. (2018) Geochemical impacts of hydrothermal activity on surface deposits at the Southwest Indian Ridge. *Deep Sea Res. Part I* **139**, 1–13.

Peacock C. L. and Sherman D. M. (2004) Vanadium(V) adsorption onto goethite (α-FeOOH) at pH 1.5 to 12: a surface complexation model based on ab initio molecular geometries and EXAFS spectroscopy. *Geochim. Cosmochim. Acta* **68**, 1723–1733.

Piper D. Z. and Dean W. E. (2002) *Trace-element deposition in the Cariaco Basin, Venezuela Shelf, under sulfate-reducing conditions: a history of the local hydrography and global climate, 20 ka to the present*. Professional Paper, Reston, VA, p. 41.

Planavsky N., Bekker A., Rouxel O. J., Kamber B., Hofmann A., Knudsen A. and Lyons T. W. (2010) Rare earth element and yttrium compositions of Archean and Paleoproterozoic Fe formations revisited: new perspectives on the significance and mechanisms of deposition. *Geochim. Cosmochim. Acta* **74**(22), 6387–6405.

Pokrovsky O. S., Viers J. and Freydier R. (2005) Zinc stable isotope fractionation during its adsorption on oxides and hydroxides. *J. Colloid Interface Sci.* **291**, 192–200.

Prytulak J., Nielsen S. G. and Halliday A. N. (2011) Determination of Precise and Accurate 51V/50V Isotope Ratios by Multi-Collector ICP-MS, Part 2: Isotopic Composition of Six Reference Materials plus the Allende Chondrite and Verification Tests. *Geostand. Geoanal. Res.* **35**, 307–318.

Prytulak J., Nielsen S. G., Ionov D. A., Halliday A. N., Harvey J., Kelley K. A., Niu Y. L., Peate D. W., Shimizu K. and Sims K. W. W. (2013) The stable vanadium isotope composition of the mantle and mafic lavas. *Earth Planet. Sci. Lett.* **365**, 177–189.

Radford-Knoery J., German C., Charlou J.-L., Donval J.-P. and Fouquet Y. (2001) Distribution and behavior of dissolved hydrogen sulfide in hydrothermal plumes. *Limnol. Oceanogr.* **46**, 461–464.

Rasmussen B., Krapež B., Muhling J. R. and Suvorova A. (2015) Precipitation of iron silicate nanoparticles in early Precambrian oceans marks Earth's first iron age. *Geology* **43**(4), 303–306.

Resing J. A., Sedwick P. N., German C. R., Jenkins W. J., Moffett J. W., Sohst B. M. and Tagliabue A. (2015) Basin-scale transport of hydrothermal dissolved metals across the South Pacific Ocean. *Nature* **523**, 200–203.

Richter F. M., Rowley D. B. and DePaolo D. J. (1992) Sr isotope evolution of seawater: the role of tectonics. *Earth Planet. Sci. Lett.* **109**, 11–23.

Rolison J. M., Stirling C. H., Middag R. and Rijkenberg M. J. (2017) Uranium stable isotope fractionation in the Black Sea: Modern calibration of the 238 U/235 U paleo-redox proxy. *Geochim. Cosmochim. Acta*.

Rona P. A., Bogdanov Y. A., Gurvich E. G., Rimski-Korsakov N. A., Sagalevitch A. M., Hannington M. D. and Thompson G. (1993) Relict hydrothermal zones in the TAG hydrothermal field, Mid-Atlantic Ridge 26° N, 45° W. *J. Geophys. Res. Solid Earth* **98**, 9715–9730.

Rudnick R. and Gao S. (2003) Composition of the continental crust. *Treat. Geochem.* **3**, 1–64.

Rudnicki M. and Elderfield H. (1993) A chemical model of the buoyant and neutrally buoyant plume above the TAG vent field, 26 degrees N, Mid-Atlantic Ridge. *Geochim. Cosmochim. Acta* **57**, 2939–2957.

Sander S. G. and Koschinsky A. (2011) Metal flux from hydrothermal vents increased by organic complexation. *Nat. Geosci.* **4**, 145–150.

Sands C. M. (2006) *Hydrothermal plumes and processes in Indian Ocean*. University of Southampton.

Schaller T., Morford J., Emerson S. R. and Feely R. A. (2000) Oxyanions in metalliferous sediments: tracers for paleoseawater metal concentrations? *Geochim. Cosmochim. Acta* **64**, 2243–2254.

Scholz F., Hensen C., Noffke A., Rohde A., Liebetrau V. and Wallmann K. (2011) Early diagenesis of redox-sensitive trace metals in the Peru upwelling area–response to ENSO-related oxygen fluctuations in the water column. *Geochim. Cosmochim. Acta* **75**, 7257–7276.

Schuth S., Brüske A., Hohl S. V., Jiang S.-Y., Meinhardt A.-K., Gregory D. D., Viehmann S. and Weyer S. (2019) Vanadium and its isotope composition of river water and seawater: Analytical improvement and implications for vanadium isotope fractionation. *Chem. Geol.* **528**, 119261.

Schuth S., Horn I., Brüske A., Wolff P. E. and Weyer S. (2017) First vanadium isotope analyses of V-rich minerals by femtosecond laser ablation and solution-nebulization MC-ICP-MS. *Ore Geol. Rev.* **81**, 1271–1286.

Severmann S., Johnson C., Beard B., German C., Edmonds H., Chiba H. and Green D. (2004) The effect of plume processes on the Fe isotope composition of hydrothermally derived Fe in the deep ocean as inferred from the Rainbow vent site, Mid-Atlantic Ridge, 36 14′ N. *Earth Planet. Sci. Lett.* **225**, 63–76.

Severmann S., Mills R. A., Palmer M. R., Telling J. P., Cragg B. and Parkes R. J. (2006) The role of prokaryotes in subsurface weathering of hydrothermal sediments: a combined geochemical and microbiological investigation. *Geochim. Cosmochim. Acta* **70**(7), 1677–1694.

Seyfried W. E. and Mottl M. J. (1982) Hydrothermal alteration of basalt by seawater under seawater-dominated conditions. *Geochim. Cosmochim. Acta* **46**, 985–1002.

Shiller A. M. and Mao L. J. (2000) Dissolved vanadium in rivers: effects of silicate weathering. *Chem. Geol.* **165**, 13–22.

Thompson G., Mottl M. J. and Rona P. A. (1985) Morphology, mineralogy and chemistry of hydrothermal deposits from the TAG area, 26 N Mid-Atlantic Ridge. *Chem. Geol.* **49**, 243–257.

Toner B. M., Fakra S. C., Manganini S. J., Santelli C. M., Marcus M. A., Moffett J. W., Rouxel O., German C. R. and Edwards K. J. (2009) Preservation of iron (II) by carbon-rich matrices in a hydrothermal plume. *Nat. Geosci.* **2**, 197–201.

Trefry J. H. and Metz S. (1989) Role of hydrothermal precipitates in the geochemical cycling of vanadium. *Nature* **342**, 531–533.

Trocine R. P. and Trefry J. H. (1988) Distribution and chemistry of suspended particles from an active hydrothermal vent site on the Mid-Atlantic Ridge at 26 N. *Earth Planet. Sci. Lett.* **88**, 1–15.

Waeles M., Cotte L., Pernet-Coudrier B., Chavagnac V., Cathalot C., Leleu T., Laës-Huon A., Perhirin A., Riso R. and Sarradin P. M. (2017) On the early fate of hydrothermal iron at deep-sea vents: A reassessment after in situ filtration. *Geophys. Res. Lett.* **44**, 4233–4240.

Wasylenki L. E., Swihart J. W. and Romaniello S. J. (2014) Cadmium isotope fractionation during adsorption to Mn oxyhydroxide at low and high ionic strength. *Geochim. Cosmochim. Acta* **140**, 212–226.

Wheat C. G., Mottl M. J. and Rudnicki M. (2002) Trace element and REE composition of a low-temperature ridge-flank hydrothermal spring. *Geochim. Cosmochim. Acta* **66**, 3693–3705.

Wu F., Owens J. D., Huang T., Sarafian A., Huang K.-F., Sen I. S., Horner T. J., Blusztajn J., Morton P. and Nielsen S. G. (2019a) Vanadium isotope composition of seawater. *Geochim. Cosmochim. Acta* **244**, 403–415.

Wu F., Owens J. D., Scholz F., Huang L., Li S., Riedinger N., Peterson L. C., German C. R. and Nielsen S. G. (2020) Sedimentary vanadium isotope signatures in low oxygen marine conditions. *Geochim. Cosmochim. Acta* **284**, 134–155.

Wu F., Owens J. D., Tang L., Dong Y. and Huang F. (2019b) Vanadium isotopic fractionation during the formation of marine ferromanganese crusts and nodules. *Geochim. Cosmochim. Acta* **265**, 371–385.

Wu F., Qi Y., Perfit M. R., Gao Y., Langmuir C. H., Wanless V. D., Yu H. and Huang F. (2018) Vanadium isotope compositions of mid-ocean ridge lavas and altered oceanic crust. *Earth Planet. Sci. Lett.* **493**, 128–139.

Wu F., Qi Y., Yu H., Tian S., Hou Z. and Huang F. (2016) Vanadium isotope measurement by MC-ICP-MS. *Chem. Geol.* **421**, 17–25.

Wu F., Qin T., Li X., Liu Y., Huang J.-H., Wu Z. and Huang F. (2015) First-principles investigation of vanadium isotope fractionation in solution and during adsorption. *Earth Planet. Sci. Lett.* **426**, 216–224.

Associate editor: Noah J. Planavsky